Quaternary Science Reviews 316 (2023) 108253

Contents lists available at ScienceDirect

Quaternary Science Reviews

journal homepage: www.elsevier.com/locate/quascirev

# Eccentricity signal in the nannofossil time-series across the Mid-Pleistocene Transition in the northwestern Pacific Ocean (ODP Site 1209)

Manuela Bordiga [a,b], Claudia Lupi [b,*], Roberto Sacchi [b], Patrizia Ferretti [c], Simon J. Crowhurst [d], Miriam Cobianchi [b]

[a] National Institute of Oceanography and Applied Geophysics, Via Auguste Piccard 54, 34151, Trieste, Italy
[b] Department of Earth and Environmental Sciences, University of Pavia, Via Ferrata 1, 27100, Pavia, Italy
[c] Department of Environmental Sciences, Informatics and Statistics, Ca' Foscari University of Venice, Via Torino 155, 30170, Venezia Mestre, Italy
[d] The Godwin Laboratory for Palaeoclimate Research, Department of Earth Sciences, University of Cambridge, Downing Street, Cambridge, CB2 3EQ, United Kingdom

ARTICLE INFO

Handling editor: A. Voelker

*Keywords:*
Calcareous nannofossils
Mid-Pleistocene transition
Orbital cycles
Eccentricity
Wavelet analysis
Autocorrelation
Cross-correlation
Northwest Pacific Ocean

ABSTRACT

The Mid-Pleistocene Transition (MPT; 1.25–0.6 million years ago, Ma) is one of the most important and still debated climate reorganizations during which the glacial/interglacial cycles switched from a 41-thousand years (kyr) cycle (i.e. obliquity) to a quasi-periodic 100-kyr cycle (associated with orbital eccentricity). Variations in the orbital geometry can affect the abundance and distribution of certain marine biota such as the coccolithophores, a group of unicellular calcifying phytoplankton, whose skeletal remains – called nannofossils – represent a valid tool within the geological archives to infer change in surface water conditions and/or coccolithophore productivity and how orbital variations may have impacted them. Here, we apply for the first time various time series analytical techniques to the nannofossil dataset from mid-latitudinal Ocean Drilling Program (ODP) Site 1209 in the northwest Pacific Ocean for the interval spanning the last 1.6 Myr. To better interpret the orbital signal recorded by different nannofossil species we used time series analyses (i.e. wavelet, autocorrelation and cross correlation) to identify the main periodicities by single nannofossil species during the MPT, and to investigate further their response timings to those orbital drivers. In addition, we investigated how the recorded periodicities can improve understanding of the paleoecological preferences of particular species. The combination of multiple time series analyses allowed identification of the 100-kyr periodicity as the main cyclicity recorded in most analyzed species at Site 1209, documenting the predominance of the eccentricity-related signal at mid-latitudes and a reduced or absent influence of the obliquity response. Thus, our data highlight how orbital influence varies by latitude impacting the nannofossil species. The lag between eccentricity and species abundance fluctuations was also investigated, identifying a fast response ranging between 20 and 40 kyr for the taxa *Calcidiscus leptoporus* subspecies *leptoporus*, *Gephyrocapsa caribbeanica* small, and *Reticulofenestra* spp. (>5 μm). This study corroborates the potential of nannofossils to deepen understanding of the dynamics and effects of variations in orbital geometry through time. It also underlines the need to extend the study of the responses of specific species through the use of different time series analysis techniques in order to return complementary information and detect clearer orbital signals.

## 1. Introduction

The Mid-Pleistocene Transition (MPT), between approximately 1.25 and 0.65 Ma (Clark et al., 2006; Lupi et al., 2019; Mudelsee and Schulz, 1997), represents the period when the climate periodicity changed from a dominant 41-kyr cyclicity related to orbital obliquity to a 100-kyr cyclicity associated with orbital eccentricity (Berger and Jansen, 1994; Clark et al., 1999; Mudelsee and Schulz, 1997; Shackleton and Opdyke, 1976). Hypotheses on MPT drivers and modes are still debated (Berends et al., 2021). The MPT is considered a gradual process during which the alteration in the climatic periodicity was accompanied by various local and global changes in the climate system, including lower global temperatures, increased global ice volume, lower sea-surface temperatures, more intense glaciations and perturbations of the thermohaline

* Corresponding author.Department of Earth and Environmental Sciences, University of Pavia, Via Ferrata 1, 27100, Pavia, Italy.
*E-mail addresses:* mbordiga@ogs.it (M. Bordiga), claudia.lupi@unipv.it (C. Lupi), roberto.sacchi@unipv.it (R. Sacchi), patrizia.ferretti@unive.it (P. Ferretti), patrizia.ferretti@unive.it (S.J. Crowhurst), miriam.cobianchi@unipv.it (M. Cobianchi).

https://doi.org/10.1016/j.quascirev.2023.108253
Received 21 December 2022; Received in revised form 28 July 2023; Accepted 28 July 2023

circulation after 950 ka (Clark et al., 2006; Kitamura and Kawagoe, 2006; Lisiecki and Raymo, 2007; Pisias and Moore, 1981; Prell, 1982; Sexton and Barker, 2012; Shackleton et al., 1990). Some researchers have highlighted the occurrence of abrupt events during the MPT (Elderfield et al., 2012; Lupi et al., 2019) that indicate different responses among various latitudes and oceans. The influence of high-latitude sea-ice dynamics has been inferred as the main driver for the MPT (Berends et al., 2021; Clark et al., 2006; Elderfield et al., 2012; Huybers and Wunsch, 2005), but the peculiar response of mid- and low-latitudes to orbital cycles has invoked other possible drivers such as atmospheric circulation (Lupi et al., 2019; McClymont et al., 2013), atmospheric carbon dioxide content ($CO_{2atm}$) (Lee and Poulsen, 2005; Medina-Elizalde and Lea, 2005), temperature variations in the Western Pacific Warm Pool (de Garidel-Thoron et al., 2005), or a weakening of the thermohaline circulation (Pena and Goldstein, 2014).

After the MPT, the 100-kyr cyclicity is the most powerful Milankovitch periodicity recorded worldwide following the "900-ka event", as documented by several studies focusing on different proxies (Beaufort et al., 2022; Clark et al., 2006; Cobianchi et al., 2012; Ford and Raymo, 2019; McClymont et al., 2013; Medina-Elizalde and Lea, 2005; Rickaby et al., 2007). In contrast, the obliquity (41-kyr) and precession (23-kyr) frequencies seem to record generally a more latitudinally related signal. Specifically, obliquity is more evident at high latitudes (Lee and Poulsen, 2005; Marino et al., 2009; Medina-Elizalde and Lea, 2005; Ruddiman et al., 1986; Tabor et al., 2015), whereas the strongest precessional signal is recorded at low latitudes (e.g. Ao et al., 2012; Beaufort et al., 2001).

To investigate the orbital periodicities characterizing the MPT and the responses of the climate system, it is important to select continuous archives sampled at high-resolution. The most useful archives are the ice cores of Vostok and EPICA, providing high-resolution records of $CO_2$, methane, and the stable isotopes of deuterium and oxygen; however, their temporal span is currently limited to the last 800 kyr (EPICA community members, 2004; Jouzel et al., 2007; Petit et al., 1999; Siegenthaler et al., 2005). Thus, they do not provide any data from before the MPT. On the other hand, marine sediments provide extended temporal and spatial coverage, although at generally lower resolution than the ice cores. So far, many studies examining the MPT use foraminiferal stable isotope measurements (Berger et al., 1994; Cobianchi et al., 2012; de Garidel-Thoron et al., 2005; Diekmann and Kuhn, 2002; Elderfield et al., 2012; Hodell and Channell, 2016; Weirauch et al., 2008), whereas fewer studies examine nannofossil assemblages across the entire MPT with sufficient temporal resolution and duration to investigate orbital cyclicity (Beaufort et al., 2022; Jin et al., 2022; Lupi et al., 2019). However, since coccolithophores are sensitive indicators of environmental conditions (e.g. Winter et al., 1994), the nannofossil assemblages may record variations related to the orbital cycles recorded in the geological archives, as demonstrated for example by Beaufort et al. (2022), Marino et al. (2009), and Rickaby et al. (2007). To date, the response to Milankovitch cycles recorded by several proxies in marine sediments has been mainly investigated at higher southern latitudes (e.g. Diekmann and Kuhn, 2002; Lisiecki and Raymo, 2007; Marino et al., 2009) and northern latitudes (Hodell and Channell, 2016; Martínez-Sánchez et al., 2019; Ruddiman et al., 1986) in the Atlantic Ocean. In the Pacific Ocean, the orbital periodicities linked to the MPT have been investigated at middle and equatorial latitudes (Beaufort et al., 2022; Berger et al., 1994; Cobianchi et al., 2012; Medina-Elizalde and Lea, 2005; Weirauch et al., 2008). Only one recent study investigated at high resolution the nannofossil response to astronomical periodicities and their variation through time across the last 2.8 Myr at mid- and low-latitudes (Beaufort et al., 2022).

The mid-latitude site presented here, Ocean Drilling Program (ODP) Site 1209 located in the NW Pacific Ocean, has never been previously investigated for orbital periodicities in the nannofossil record over the last 1.6 Myr and represents one of the few long records investigated at this latitude. Prell (1982, 2013) established the presence of 100-kyr periodicities in paleoproductivity and nannofossil calcium carbonate ($CaCO_3$) accumulation derived from nannofossil analyses, but only for the last 450 kyr. More recently, Lupi et al. (2019) studied the calcareous nannofossil content at ODP Site 1209 from 400 to 1500 ka through multivariate analysis, highlighting that nannofossils documented three different associations related to the pre-MPT (older than 1250 ka), the MPT (1250-621 ka), and post-MPT (younger than 621 ka). These authors demonstrated that abrupt changes in the nannofossil species frequency and diversity across the MPT boundaries overlapped with a long term, gradual trend without a clear correlation with glacial/interglacial oscillations. In addition, they also documented a peculiar change in the nannofossil assemblages centered at 900 ka. Building on these previous studies, we conducted wavelet and time series analyses on the nannofossil distribution data to establish: i) the orbital influence on nannofossil assemblage composition and abundance, including cyclicity and timing, and ii) if the recorded orbital signal can help to improve understanding of nannoplankton ecological response to climate change.

## 2. Oceanographic setting

ODP Site 1209 (Leg 198; 32°39.1081′N, 158°30.3564′E) was drilled at a bathyal water depth of 2387 m on the Southern High of the Shatsky Rise (Bralower et al., 2002), a plateau located 1600 km east of Japan in the subtropical region of the NW Pacific Ocean (Fig. 1). In this region of the Pacific Ocean, the lysocline is shallower than 2900 m depth (Vincent, 1975) and the calcite compensation depth (CCD) is between 4000 and 4500 m depth (Berger and Winterer, 1974). The studied site is located in the subtropical climatic region, within a transitional zone between the subtropical and the subarctic oceanic gyres (Fig. 1A), making it sensitive to climate changes (e.g. Haug et al., 1995; Kawahata et al., 1999; Sancetta and Silvestri, 1986; Thompson, 1981; Thompson and Shackleton, 1980). Currently, the surface oceanography is characterized by two main currents (Fig. 1B): the subtropical warm oligotrophic Kuroshio Current from the south, and the subarctic cold and eutrophic Oyashio Current from the north (Kawahata et al., 1999; Kawahata and Ohshima, 2002; Qiu, 2001). The positions and intensity of these two currents strongly influence the climate conditions and primary productivity of the NW Pacific Ocean (Liu et al., 2004; Qiu, 2000, 2002; Sasai, 2007). In particular, the Kuroshio is the most powerful western boundary current in the North Pacific (e.g. Hu et al., 2015; Qiu, 2002, 2001; Usui et al., 2013) with a width of ca. 100 km and a maximum depth of 1 km (Barkley, 1970).

## 3. Material and methods

### 3.1. ODP Site 1209: age model

An accurate age model is pivotal for studying the orbital signals recorded within geological time series. Thus, we revised the previously published age models of the last 1.6 Myr for ODP Site 1209, along a sequence spanning from 0 to 22 m below sea floor (mbsf), i.e. 0.12–22.61 m composite depth (mcd) (for the revised mcd refer to Westerhold and Röhl, 2006). The previous age models were mainly based on calcareous nannofossil biostratigraphy (Lupi et al., 2012, 2019); whereas the foraminiferal isotope stratigraphy, and thus a better constrained age model, is available only for the last 450 kyr (Bordiga et al., 2013, 2014). Due to the lack of isotopic data at the studied site in the older part of our record, we used a different dataset as reference for the age model tuning. We selected the color reflectance parameter lightness (L*) record collected shipboard using a Minolta spectrophotometer (model CM-2002) (Bralower et al., 2002). At the top of the sedimentary sequence recovered from ODP Site 1209 (0–1.525 mbsf, 0.12–1.645 mcd), onboard reflectance data were not available; for this reason, we extracted L*, redness (a*) and blueness (b*) records from core images taken during the expedition using the Avaatech XRF-scanner image software. Then, regression analyses were performed on the newly reconstructed datasets in order to rescale and compare them to the same parameters measured onboard. The results of this

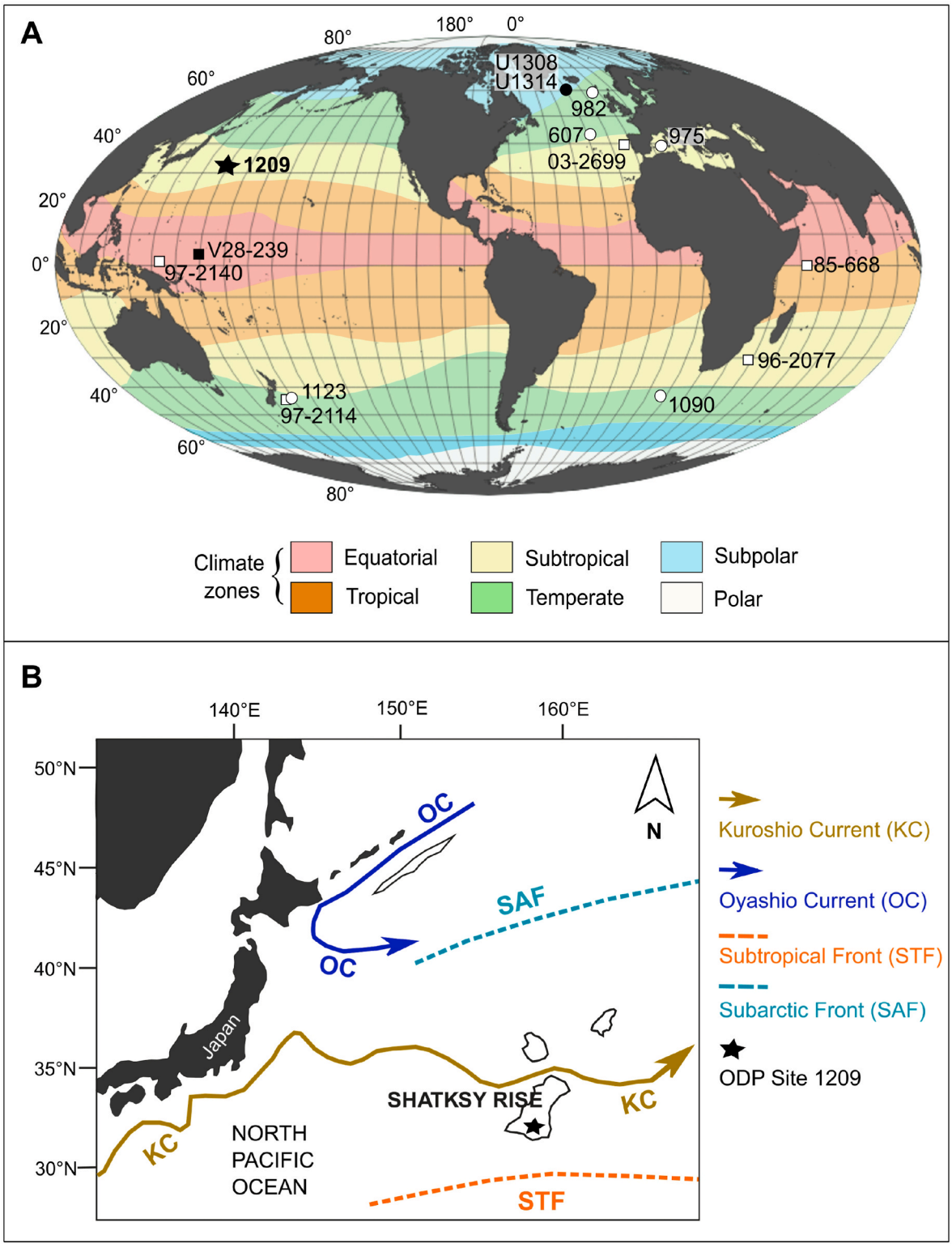


**Fig. 1.** A) Locations of ODP Site 1209 (black star) and the sites cited for comparison: Ocean Drilling Program (ODP) sites (white circles); International Ocean Discovery Program (IODP) site (black circle); MD cores drilled by the International Marine Past Global Change Study (IMAGES) cruises (white squares); core recovered by the research vessel R/V Vema (black square). The oceanic climatic regions are also displayed and identified by different colors (modified from Trujillo and Thurman, 2011). Map is outlined using worldmapgenerator (Stirnemann and Bühlmann, 2021). B) Geographical position of the studied ODP Site 1209 on the Shatsky Rise, together with the trajectory of the main currents, Kuroshio and Oyashio, and the position of the Subtropical and Subarctic Fronts (modified from Kawahata and Ohshima, 2002).

comparison for the L* records are shown in Fig. 2A, demonstrating that there is an excellent match between the L* measured onboard and the L* reconstructed using the core images, giving us confidence that the latter could be used for age model development. The age model was reconstructed by tuning the L*-scanned curve to the benthic $\delta^{18}O$ stack LR04 of Lisiecki and Raymo (2005). Lighter colors, thus intervals with a higher content of $CaCO_3$, were correlated with lighter $\delta^{18}O$ values characterizing the interglacial phases. As each version of the age model was developed, we performed wavelet analyses of both our L* record and the tuning target, in order to evaluate the proportion of the variance in the tuned record that might be attributable by linear forcing related to the target signal (Fig. 2B and C). The age control points used are shown in Fig. 2A and listed in Table 1. Following our new age model, the studied sequence spans from MIS 55 to MIS 1, covering the last ~1.6 Myr, with an average sedimentation rate of ~1.66 cm $kyr^{-1}$, comparable to the sedimentation rates and age model published in Lupi et al. (2019). The sample spacing provides a resolution of at least 7.3 kyr along the overall studied interval.

### 3.2. ODP Site 1209: nannofossil samples and assemblage data

The Pleistocene succession at ODP Site 1209 is complete and continuous, and it consists largely of nannofossil ooze and nannofossil ooze with clay (up to 70% $CaCO_3$ by weight), with foraminifera, diatoms and radiolarians as minor components (Bordiga et al., 2013; Bralower et al., 2002; Lupi et al., 2012). From ODP Site 1209, we processed 251 samples between 0 and 22 mbsf (0.12–22.61 mcd) with a sampling resolution spanning from 5 to 10 cm (i.e. from 3.8 kyr to 7.3 kyr) across the overall studied interval, with the only exception of 82 cm (i.e. 17.3 kyr) gap between Cores 1209-2H and 1209-3H (see dataset in Zenodo, https://doi.org/10.5281/zenodo.8191622). Relative abundances of nannofossil species for 218 samples are from previously published works (Bordiga et al., 2013, 2014; Lupi et al., 2012, 2019), whereas 33 samples (11.45–14.55 mbsf; 11.39–14.49 mcd) have been newly studied for their nannofossil content increasing the temporal resolution across the MPT to ~3.8 kyr. The newly studied samples were prepared following the drop technique (Bordiga et al., 2015), which allows calculating relative (%) and absolute (N $g^{-1}$) abundances of the species, in order to compare the reliability of both datasets. These samples were analyzed under a Leitz 12 POL, polarizing light microscope (1000X). More than 500 specimens encountered in at least 20 fields of view were distinguished at species level following the calcareous nannofossil taxonomy reported in Nannotax3 (edited by Young et al., 2022). For details of the morphological characterization of the *Gephyrocapsa* group see Lupi et al. (2012). The *Reticulofenestra* spp. (>5 μm) group also includes the morphotypes intermediate between *Reticulofenestra* (>5 μm) and *Pseudoemiliania* (>5 μm) characterized by only few slits visible on the distal shield (cf. Maiorano and Marino, 2004).

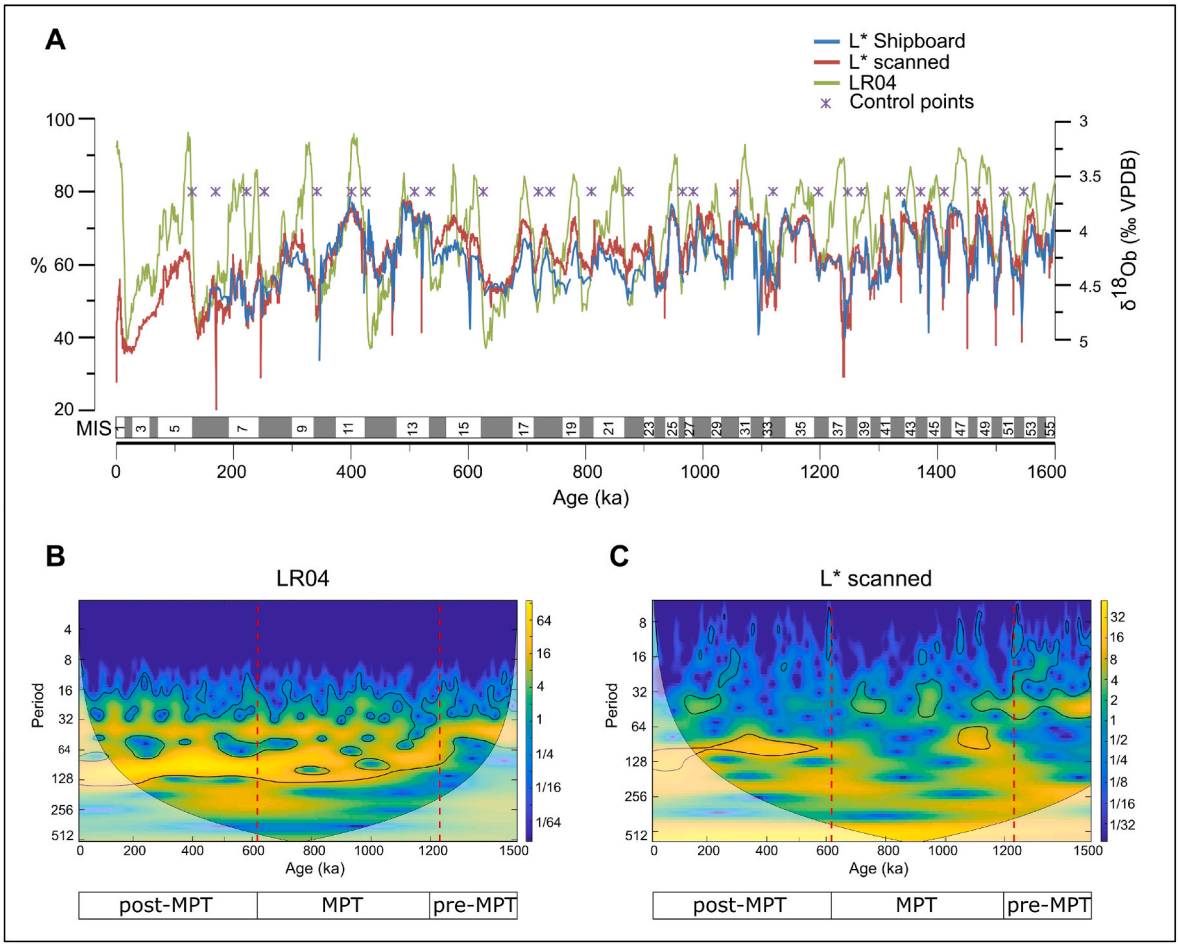


**Fig. 2.** A) Age model for ODP Site 1209 developed using the lightness (L*) measured in percentage (%) on the core images (red curve) and the L* collected onboard (blue curve) by the Shipboard Party (Bralower et al., 2002) plotted against the $\delta^{18}O_b$ LR04 reference stack (green curve; Lisiecki and Raymo, 2005). The control points (purple crosses) used in this work for the age model calibration are shown. Marine Isotope Stage (MIS) numbers indicative of the interglacial phases are reported, whereas the grey boxes represent the glacial phases. B–C) Wavelet analyses of LR04 curve (B) and L* scanned at ODP Site 1209 (C). All the data were interpolated at constant 7 kyr intervals, with an 18 kyr gaussian window. Black lines outline the 95% confidence level. The three time intervals taken as reference (pre-MPT, MPT, and post-MPT) are reported following Lupi et al. (2019) and highlighted by red dotted lines.

**Table 1**
Control points identified in this work; mbsf: meters below sea floor (Bralower et al., 2002); mcd: meter composite depth (Westerhold and Röhl, 2006).

| # key point | mbsf | mcd | control age (ka) |
|---|---|---|---|
| 1 | 0 | 0.12 | 0 |
| 2 | 0.15 | 0.28 | 19 |
| 3 | 0.33 | 0.45 | 60 |
| 4 | 1.2 | 1.32 | 130 |
| 5 | 1.6 | 1.72 | 170 |
| 6 | 2.63 | 2.75 | 250 |
| 7 | 4 | 4.12 | 343 |
| 8 | 5.17 | 5.11 | 429 |
| 9 | 7.8 | 7.74 | 505 |
| 10 | 8.45 | 8.39 | 536 |
| 11 | 9.48 | 9.42 | 626 |
| 12 | 10.27 | 10.21 | 720 |
| 13 | 10.5 | 10.44 | 740 |
| 14 | 11.02 | 10.96 | 810 |
| 15 | 11.8 | 11.74 | 874 |
| 16 | 13 | 12.94 | 966 |
| 17 | 13.1 | 13.04 | 985 |
| 18 | 14.05 | 13.99 | 1055 |
| 19 | 14.83 | 15.43 | 1120 |
| 20 | 15.44 | 16.05 | 1198 |
| 21 | 15.94 | 16.55 | 1248 |
| 22 | 16.17 | 16.78 | 1270 |
| 23 | 17.57 | 18.18 | 1338 |
| 24 | 18.25 | 18.86 | 1372 |
| 25 | 18.95 | 19.56 | 1412 |
| 26 | 19.8 | 20.41 | 1466 |
| 27 | 20.67 | 21.28 | 1513 |
| 28 | 21.37 | 21.98 | 1548 |

To investigate the presence and distribution of orbital cycles within the nannofossil assemblages, we processed the data derived from the six most abundant species across the MPT – i.e. *C. leptoporus* subsp. *leptoporus*, *Florisphaera profunda*, *Gephyrocapsa caribbeanica* small (<4 μm), *Gephyrocapsa ericsonii*, *Pseudoemiliana lacunosa*, *Reticulofenestra* spp. (>5 μm) (Fig. 3). Details on the assemblages at ODP Site 1209 have been already published in Bordiga et al. (2013, 2014), and Lupi et al. (2012, 2019). At the studied site the $CaCO_3$ (w%t) content is high (from 89 to 35 wt%, average value 68 wt%) along the whole studied sequence with only two samples having low carbonate content. The preservation of the nannofossil assemblages is usually good with many fluctuations in the last 1.6 Myr, as shown by the Nannofossil Dissolution Index (NDI). The diversity (H index) records the lowest values in the oldest samples (average value 2.19), whereas after 1.45 Ma until 520 ka the diversity gradually increases (average: 2.53; maximum: 2.95). After, other two intervals show significant decreases in diversity (i.e. from 520 to 485 ka, and between 400 and 300 ka), followed by a recover after 300 ka (average value 2.7) where the H index also reaches its maximum value (Fig. 3). One of the most abundant species in the pre- and post-MPT, especially from 560 to 250 ka, is *G. caribbeanica* small that reaches up to an average of 65% in the latter interval. During the MPT the most abundant species are *P. lacunosa* and *Reticulofenestra* spp. (>5 μm) which represent ca. 25% of the entire assemblage from 1250 to 600 ka (Fig. 3). It is notable, that those two taxa disappear from the assemblages around 460 ka, whereas the small reticulofenestrids (coccolith size <5 μm) are present in younger sediments. *Gephyrocapsa ericsonii* also brings a significant contribution to the pre-MPT assemblages and along the entire MPT, reaching up to 40% in some intervals, but its abundance decreases after 450 ka (Fig. 3). Other species that contribute to the nannofossil assemblages at Site 1209 but that are not discussed here are: *Gephyrocapsa aperta* which has a higher abundance (up to 50%) only after 200 ka, *Gephyrocapsa oceanica*, *Coccolithus pelagicus*, *Helicosphaera* spp., and *Rhabdosphaera clavigera*. For more details on the abundance and distribution of these taxa see previously published works (Bordiga et al., 2014; Lupi et al., 2012, 2019).

The relative and absolute abundances available for the newly studied samples have been used to verify the consistency through time of the abundance fluctuations detectable through the two different datasets. By performing the Pearson correlation coefficient among the relative and absolute abundances of the six selected species we document a strict relationship between the two datasets, obtaining correlation values from excellent (e.g. 0.98, 0.94, 0.91 for *G. ericsonii*, *G. caribbeanica* small, and *Reticulofenestra* spp. (>5 μm) respectively) to very good (e.g. 0.73 for *P. lacunosa*), with an average correlation among all species of 0.84 (Table S1).

To better interpret and discuss the results in relation to understanding nannofossil paleoecological preferences, we considered the most recent and acknowledged literature for the species selected in this work (Table 2).

### 3.3. Wavelet analyses of nannofossil species

To detect the periodicities and their distribution through time recorded at ODP Site 1209 along the last 1.6 Myr, wavelet analyses were applied over the entire record to the relative abundances of the selected nannofossil species, characterizing the pre-MPT, MPT, and post-MPT assemblages as highlighted by Lupi et al. (2019). In particular, we analyzed *G. ericsonii* because it is one of the dominant species for the pre-MPT; for the MPT interval the main contributing taxa are *P. lacunosa*, *Reticulofenestra* spp. (>5 μm), and *C. leptoporus* subsp. *leptoporus*; whereas for the post-MPT *Gephyrocapsa caribbeanica* small is the most representative species (Lupi et al., 2019) (Fig. 3). We also processed the species *Florisphaera profunda* because it has a strong environmental significance, and it is commonly used as a paleoproductivity proxy (e.g. Beaufort et al., 1997; Flores et al., 2000; López-Otálvaro et al., 2008; Molfino and McIntyre, 1990). The wavelet plots were created using the SOWAS software package developed by Maraun et al. (2007) and Maraun and Kurths (2004). Before analyses, data were interpolated to 7 kyr intervals using an 18 kyr Gaussian window.

### 3.4. Statistical analyses of nannofossil assemblages

We applied statistical time series analyses both to summarize the cyclicity patterns over pre-MPT, MPT, and post-MPT intervals for each nannofossil species and to compare them to the 100-kyr cyclicity related to orbital eccentricity over the same time interval. As reference eccentricity time series, we used Laskar et al. (2011). The time series analytical technique used here evaluates the time lag between two consecutive values as constant throughout the entire analyzed time interval. To do this, we resampled each series (e.g. nannofossil species and eccentricity) at an interval of 7.3 kyr, corresponding to the mean time lag between two consecutive measures computed over the whole data set (Fig. S1). Hereafter, we used min-max normalization in order to scale the observed values of each series into a range between 0 and 1 to make them more directly comparable to each other. We used an autocorrelation function (ACF) to provide insight into the oscillatory processes underlying the series, as well as to detect the frequency of the periodic fluctuations of each time series. Then, we used a cross-correlation function (CCF) to analyze the relationship between the 100-kyr cyclicity of orbital eccentricity and the cyclicity of each nannofossil series. Since we were looking for possible leading (i.e. predictive) effects of the eccentricity on nannofossil species, only negative lags were considered. Negative values indicate that the variation in maximum eccentricity precedes changes in species abundances (i.e. maximum eccentricity predicts species variation). In contrast, positive values mean the opposite, i.e. the fluctuation in species abundances precedes variation in eccentricity, which is not consistent with a simple view of the effects of orbital eccentricity on biological variation.

Finally, we used lag linear regression models in order to detect the lags at which the relationships between eccentricity and nannofossil abundances were strongest. In these analyses, the nannofossil

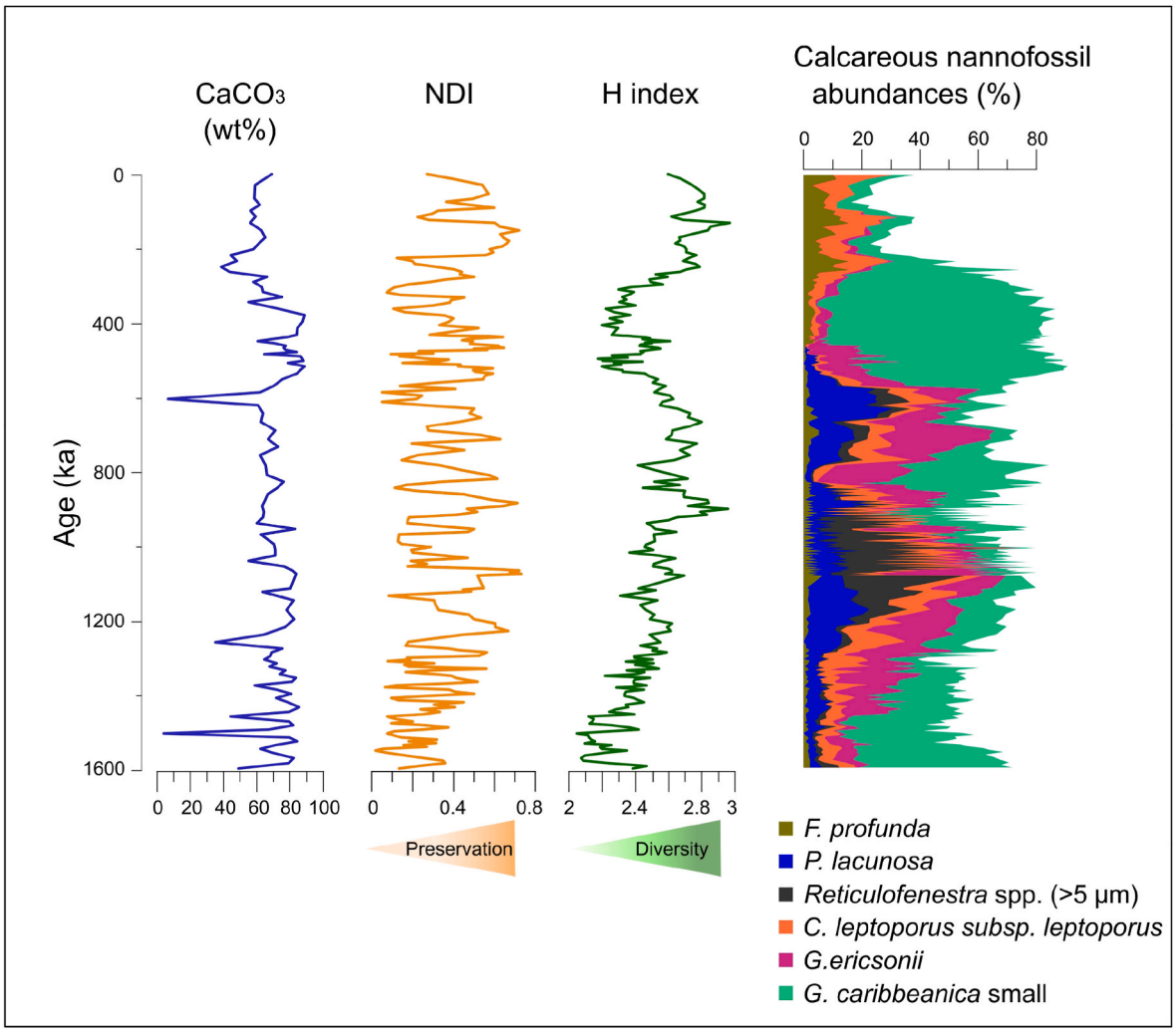


**Fig. 3.** Previously published data from Site 1209 plotted against age (ka): $CaCO_3$ (wt%) measured on bulk sediment (Lupi et al., 2012; Bordiga et al., 2013); Nannofossil Dissolution Index (NDI; Bordiga et al., 2013); H index (Lupi et al., 2012); relative abundances (%) of the selected species within the calcareous nannofossil assemblages (Bordiga et al., 2014; Lupi et al., 2012, 2019; newly collected data).

abundance was modeled as linear functions of previous lags −1 to −7 (i.e. −7.3 kyr to −51.1 kyr) relative to eccentricity. Lag 0, corresponding to synchronous measurements in the two series, was also added as a control for checking the absence of a leading effect of the eccentricity on nannofossil series. All analyses were performed in R (R Core Team, 2020) using the packages "tseries" (Trapletti and Hornik, 2020) and "astsa" (Stoffer, 2020).

**Table 2**
Summary of the main ecological tolerance and environmental preferences of the selected taxa as reported in existing literature. 1. Ziveri et al. (2004); 2. Baumann et al. (2016); 3. Renaud et al. (2002); 4. Boeckel et al. (2006); 5. Kleijne (1993); 6. Knappertsbusch et al. (1997); 7. Beaufort et al. (1997); 8. Zhang et al. (2007); 9. Okada and McIntyre (1979); 10. Okada and Honjo (1973); 11. Molfino and McIntyre (1990); 12. Saavedra-Pellitero et al. (2010); 13. Maiorano et al. (2013); 14. Baumann and Freitag (2004); 15. Marino et al. (2008); 16. Aizawa et al. (2004); 17. Winter (1982); 18. Flores et al. (1999); 19. Sprengel et al. (2002); 20. Maiorano and Marino (2004); 21. Young (1994); 22. Flores et al. (2005).

| Taxon | Ecological tolerance | Environmental preference |
|---|---|---|
| *Calcidiscus leptoporus subsp. leptoporus* | • Eutrophic conditions (1,2)<br>• Cooler water-intermediate temperature (2-4)<br>• Broad ecological tolerance (2-4) | • Cosmopolitan distribution (4-6) |
| *Florisphaera profunda* | • Water column stratification (4,7)<br>• Temperature >10°C (8,9) | • Deep dweller (10-11)<br>• Abundant when the upper photic zone is nutrient depleted (7)<br>• Subtropical stratified waters (4-7) |
| *Gephyrocapsa caribbeanica* small | • High nutrients (12,13,14) | • Upwelling areas (13,15)<br>• Cosmopolitan (14) |
| *Gephyrocapsa ericsonii* | • Warm waters >19°C (14,16-18)<br>• High nutrients (4,19) | • Tropical-temperate regions (16)<br>• Frontal systems (19) |
| *Pseudoemiliania lacunosa* | • Eutrophic conditions, high variability in salinity (15) | • Unstable environments (15) |
| *Reticulofenestra* spp. (>5 µm) | • Low salinity (20)<br>• High nutrients (15,21) | • Eutrophic and turbulent conditions (15,22)<br>• Costal and upwelling areas (21) |

## 4. Results

### 4.1. Orbital signals detectable from selected nannofossil taxa through wavelet analysis

Taking into account the sampling resolution available at ODP Site 1209, wavelet analyses were useful to identify 100-kyr and 41-kyr periodicities associated with Milankovitch cycles.

Milankovitch periodicities appear more clearly in the geological record after 1.2 Ma, thus for the MPT and post-MPT intervals, whereas the pre-MPT interval does not show any significant periodicity (Fig. 4). The most evident periodicity recorded by almost all the examined taxa, although not continuously along the entire sequence, is 100-kyr with the exception of the species *Reticulofenestra* spp. (>5 μm) and *G. caribbeanica* small (Fig. 4). It should be noted that the wavelet analysis of *P. lacunosa* and *Reticulofenestra* spp. (>5 μm) did not return any signal in the upper portion of the sedimentary sequence, because they became extinct at ca. 450 ka (Fig. 4). Strong 100-kyr power is detected in the species *P. lacunosa* between 1100 and 500 ka. *G. ericsonii* shows somewhat similar, but more complex patterns: this species gains power in this band from 1200 to 600 ka, with lower power from 1000 ka and intensified power from ~800 ka (Fig. 4). The wavelet plots of the species *F. profunda*, which has the lowest abundance of the species examined (Fig. 3), are suggestive of power at the 100-kyr periodicity mainly from 200 to 300 ka (Fig. 4). *C. leptoporus* subsp. *leptoporus* shows 100-kyr periodicity in the pre-MPT and MPT interval from just before 200 ka and later. This periodicity, however, cannot be regarded as statistically established in the youngest part of the records where power runs beyond

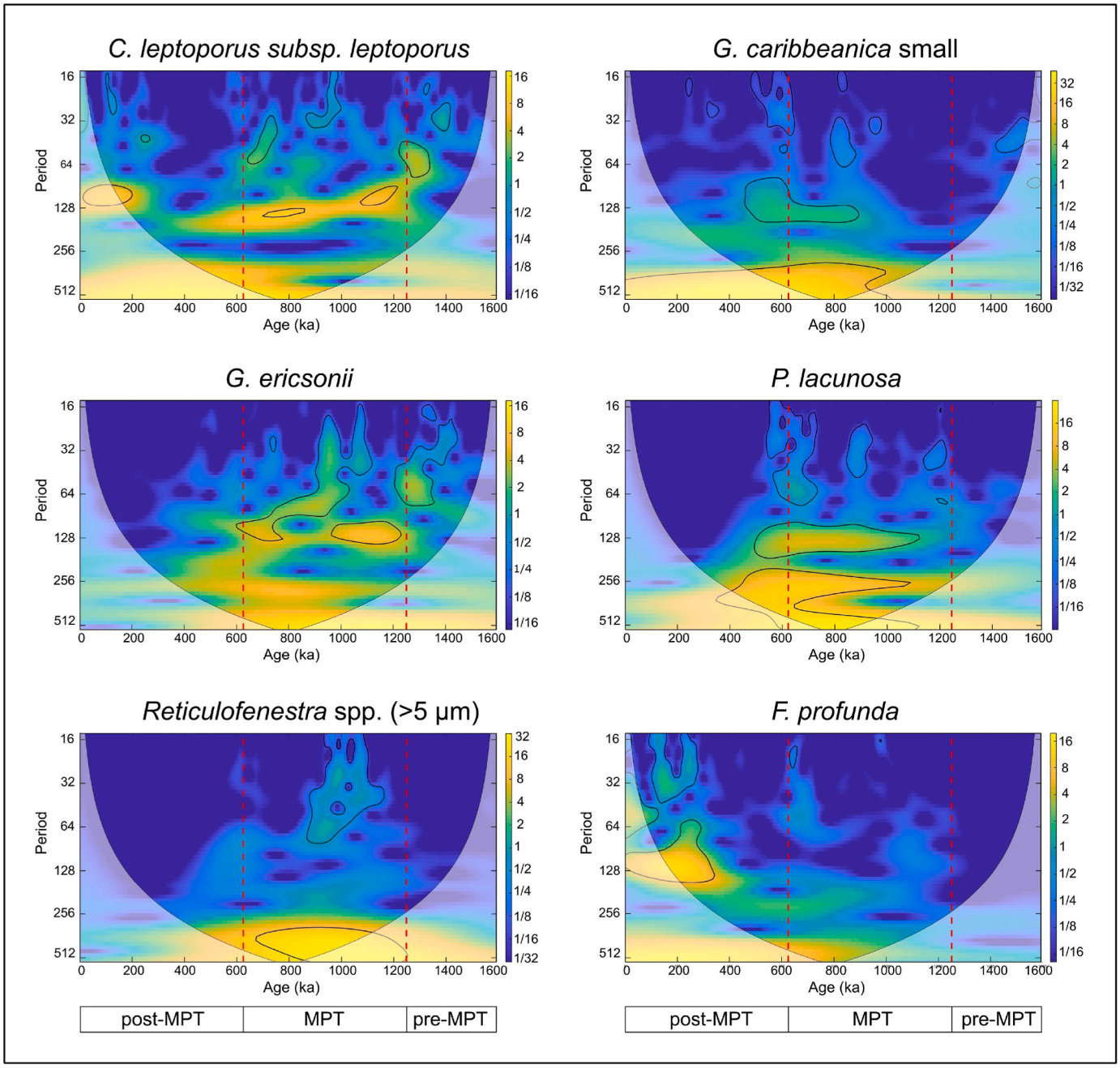


**Fig. 4.** Wavelet analyses of selected calcareous nannofossil species at ODP Site 1209. All the data were interpolated at constant 7 kyr intervals, with an 18 kyr gaussian window. Black lines outline the 95% confidence level. The pre-MPT, MPT, and post-MPT intervals are reported following Lupi et al. (2019) and highlighted by red dotted lines.

the boundaries of the cone of influence (Fig. 4). It is important to note that the duration of the studied interval is not long enough to fully resolve a complete 400-kyr cycle. Moreover, the resolution of the time series studied here makes it difficult to rule out the eccentricity amplitude modulation of precession as the ultimate source of the eccentricity-related variations described in this study. However, the long apparent lags associated with the variations in some taxa are perhaps more readily interpreted as delayed responses to eccentricity *per se* rather than to the amplitude modulation of precession.

The signals returned by the wavelet analysis are useful for informing a preliminary interpretation of the periodicities recorded in the nannofossil assemblages, but further analyses are necessary to deepen the understanding of cyclicity patterns at single species levels and to better constrain the relationships among Milankovitch periodicities and nannofossils across the MPT. To do this, we performed specific statistical treatments of our data using targeted time series analyses.

**Table 3**
Main autocorrelations in the time series of eccentricity and nannofossil relative abundances over the pre-MPT, MPT, and post-MTP intervals. Peak values correspond to the red arrows in Fig. 4C. Minimum (Min) and maximum (Max) values of the peaks together with the temporal amplitude of the correlation (N lags) are reported. One lag corresponds to 7.3 kyr, which correspond to the sampling interval.

| Series | | N lags | Peak | Min | Max |
|---|---|---|---|---|---|
| Eccentricity | 1st peak | 6 | 103 | 81 | 117 |
| | 2nd peak | 8 | 385 | 359 | 410 |
| *C. leptoporus* subsp. *leptoporus* | 1st peak | 8 | 139 | 117 | 169 |
| *Reticulofenestra* spp. (>5 μm) | 1st peak | 9 | 169 | 139 | 198 |
| *G. caribbeanica* small | 1st peak | 7 | 147 | 125 | 169 |
| *G. ericsonii* | 1st peak | 5 | 124 | 109 | 139 |
| | 2nd peak | 7 | 173 | 146 | 190 |
| *F. profunda* | 1st peak | 7 | 132 | 110 | 154 |
| *P. lacunosa* | 1st peak | 6 | 139 | 117 | 154 |

### 4.2. Statistical treatment of nannofossil abundances

The Autocorrelation function (ACF) analysis of the eccentricity time series available from Laskar et al. (2011) detected two main autocorrelations, between 81 and 117 ka (peak at 103 ka) and between 359 and 410 ka (peak at 385 ka) (Table 3; Fig. 5A), corresponding to the strongest periodicities calculated for that series. The same analysis on the six nannofossil time series showed that all species except *G. ericsonii* have a clear cyclicity (Fig. 5A and Fig. S1), with the most dominant autocorrelation between 110 and 198 ka (Table 3). *Gephyrocapsa ericsonii* shows, as the others, a clear cyclicity but with two main autocorrelations between 109 and 190 kyr (Fig. 5A; Table 3). However, the occurrence of those two peaks could be due to fluctuations in the periodicity of the series.

The cross-correlation function (CCF) analysis was able to detect significant cross-correlations for all species except *F. profunda* and *G. ericsonii* (Fig. 5B). For *F. profunda*, no significant cross-correlation was detected within the lag interval −10 (i.e. −73 kyr), whereas the most dominant cross-correlation for *G. ericsonii* occurred at lag 0, indicating that the cyclicity in eccentricity and *G. ericsonii* were nearly synchronous. Therefore, there was not any clear evidence for a leading effect of eccentricity on the abundance of these two species, at least for a time delay larger than 7.3 kyr (i.e. 1 lag). By contrast, a leading effect of the eccentricity was evident for *C. leptoporus* subsp. *leptoporus*, *Reticulofenestra* spp. (>5 μm), and *G. caribbeanica* small. A leading effect was evident also for *P. lacunosa* but the signal is less evident than in the other species, close to the threshold of non-significance (Fig. 5B). These results indicate the occurrence of a correlation in time between eccentricity and nannofossil abundance, suggesting that nannofossils respond to a change in the eccentricity, usually with a time lag. For *C. leptoporus* subsp. *leptoporus*, *Reticulofenestra* spp., and *P. lacunosa*, the most dominant cross-correlations, i.e. the dominant lags, were positive (black bars in Fig. 5B), and occurred between 51 and 14 kyr (Table 4), suggesting that an above average value of orbital eccentricity was likely to lead to

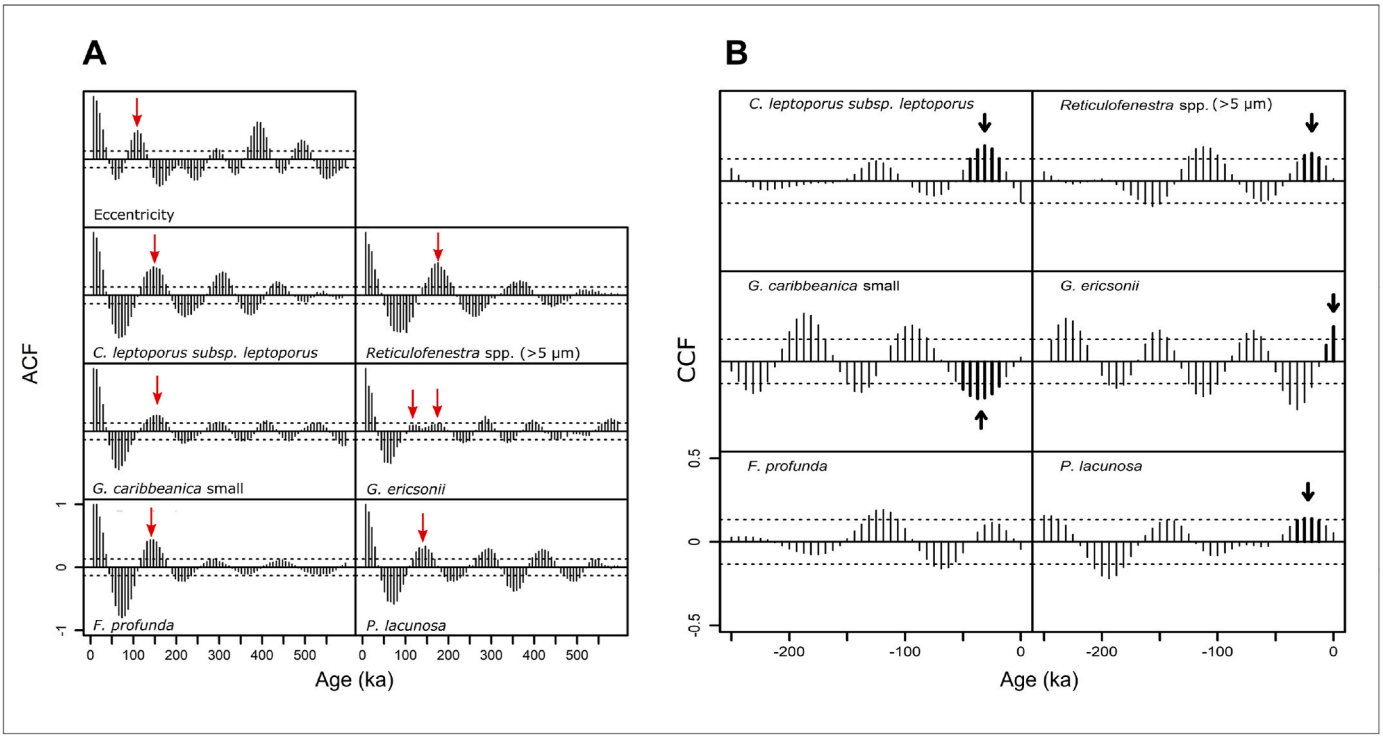


**Fig. 5.** A) Autocorrelation function (ACF) of eccentricity and the selected species revealing oscillatory processes. Dotted lines: confidence bands; red arrows: dominant autocorrelation. B) Cross-correlation function (CCF) for the relationship between each selected species and eccentricity. Dotted lines: confidence bands; black arrows: dominant cross-correlation.

**Table 4**
Dominant cross-correlations in the time series of nannofossil relative abundance by taxon with eccentricity along the MPT interval. Peak values correspond to the arrows in Fig. 5B. Minimum (Min) and maximum (Max) values of the peaks together with the temporal amplitude of the correlation (N lags) are reported. One lag unit corresponds to 7.3 kyr, which itself corresponds to the sampling interval.

| Series | N. lag | Peak | Min | Max |
|---|---|---|---|---|
| *C. leptoporus* subsp. *leptoporus* | 6 | −37 | −51 | −22 |
| *Reticulofenestra* spp. (>5 μm) | 4 | −22 | −37 | −15 |
| *G. caribbeanica* small | 7 | −40 | −66 | −22 |
| *G. ericsonii* | 6 | 11 | −7 | 29 |
| *F. profunda* | – | – | – | – |
| *P. lacunosa* | 4 | −26 | −36 | −14 |

an above average value of the nannofossil species abundance approximately 20–40 kyr later. On the other hand, the dominant cross-correlation for *G. caribbeanica* small was negative (Fig. 4D), and occurred with a lag time of between −66 and −22 kyr (Table 4). Therefore, an above average value of orbital eccentricity was likely to lead to a below average value of the *G. caribbeanica* small, approximately 40 kyr later.

Cross-correlations were substantially supported by lagged linear regression models (Table 4). Notably, we did not find any significant relationship at any lag between eccentricity and the relative abundance of *F. profunda* (Table 5). Lack of a significant relationship emerged also for *P. lacunosa* (Table 5). Consequently, the signal returned by *P. lacunosa* was not considered for further discussions. However, we found a strong relationship at lag 0 between the relative abundance of *G. ericsonii* and eccentricity, confirming the synchronicity evident in CCF analysis. In contrast, the relative abundance of *C. leptoporus* subsp. *leptoporus* significantly increased with increasing eccentricity at lag −5 and lag −4, i.e. the observations predict a peak in species abundance occurring 29.2–36.4 kyr after a peak in eccentricity (Table 5), with very similar $R^2$ coefficients (lag −5: $R^2 = 0.028$; lag −4: $R^2 = 0.029$). A similar trend was found for *Reticulofenestra* spp. (>5 μm) (Table 5), with the highest positive correlation occurring between lag −2 to lag −5, with the strongest response at lag −3 ($R^2 = 0.041$) and lag −4 ($R^2 = 0.039$). Therefore, a peak in *Reticulofenestra* spp. (>5 μm) abundance was found to occur between 21.9 kyr and 29.2 kyr after a peak in eccentricity. Finally, the abundance of *G. caribbeanica* small significantly decreased with increasing eccentricity from lag −7 to lag −3 (i.e. from −51.1 kyr to −21.9 kyr; Table 5), with the strongest response at lag −5 ($R^2 = 0.033$). Consequently, a minimum in abundance of *G. caribbeanica* small was found to occur approximately 36.5 kyr after a maximum in the eccentricity.

## 5. Discussion

### 5.1. Cyclicity reorded in fossil time series at site 1209 and worldwide

The wavelet and other time series analyses described here returned an affirmative answer to our first question as to whether the nannofossil distribution is partially controlled by orbital forcing. In fact, most of the selected nannofossil taxa mainly register eccentricity signal (100-kyr periodicity) during the MPT, and to some extent post-MPT (Figs. 4–5A), as documented by other proxies such as $\delta^{18}O$ or bulk carbonate content (e.g. Clark et al., 2006; Hodell and Channell, 2016; Sexton and Barker, 2012, Fig. 6). The only exception is *G. ericsonii,* which shows two peaks that are probably the result of two superimposed cycles (Fig. 5A). It is interesting to note that the obliquity signal (41-kyr periodicity), which is dominant at high-latitudes (e.g. Lee and Poulsen, 2005; Marino et al., 2009; Medina-Elizalde and Lea, 2005; Tabor et al., 2015), is not strongly recorded at ODP Site 1209 in the nannofossil abundance records (Figs. 4–5A). It is possible that, because of its mid-latitudinal position, the oceanographic conditions at this site are mainly influenced by low latitude ocean-atmosphere circulation, at least during and post-MPT (Bordiga et al., 2013, 2014; Lupi et al., 2019), whilst the obliquity-paced ice-sheet fluctuations did not appreciably affect the site. Finally, the precessional signal (23-kyr periodicity) cannot be identified with the available resolution (7.3 kyr) of the studied sequence.

If we focus now on the relationship between nannofossil abundances and glacial/interglacial (G-I) cycles, it looks as if the assemblages are not affected by the G-I succession. In fact, across the MPT where the periodicity of the climatic cycles is variable, the nannofossil abundances consistently record eccentricity-related variations. Therefore, they are paced by the 100-kyr orbital forcing, but not by the volume variations of the ice caps. In Lupi et al. (2019) the multivariate statistical treatment of the data collected at ODP Site 1209 supports this evidence, highlighting the observation that coccolithophores are sensitive to long-term

**Table 5**
Relationships between nannofossil abundance and eccentricity measured at lags 0 to −7, as estimated by lag linear regression models. One lag corresponds to 7.3 kyr. F: value of the F-distribution; P: p-value.

| Lag | *C. leptoporus subsp. leptoporus* | *Reticulofenestra* spp. (>5 μm) | *G. caribbeanica* small | *G. ericsonii* | *F. profunda* | *P. lacunosa* |
|---|---|---|---|---|---|---|
| lag 0 | -0.101±0.066 | 0.009±0.053 | 0.016±0.06 | **0.195±0.069** | -0.034±0.047 | 0.036±0.051 |
| 0-kyr | $F_{1,170}$=2.366 P=0.13 | $F_{1,170}$=0.032 P=0.86 | $F_{1,170}$=0.073 P=0.79 | **$F_{1,170}$=7.967 P=0.005** | $F_{1,170}$=0.52 P=0.47 | $F_{1,170}$=0.5 P=0.48 |
| lag -1 | -0.029±0.066 | 0.065±0.052 | -0.025±0.06 | 0.095±0.07 | 0.011±0.047 | 0.06±0.051 |
| -7.3-kyr | $F_{1,170}$=0.198 P=0.66 | $F_{1,170}$=1.537 P=0.22 | $F_{1,170}$=0.167 P=0.68 | $F_{1,170}$=1.834 P=0.18 | $F_{1,170}$=0.055 P=0.81 | $F_{1,170}$=1.386 P=0.24 |
| lag -2 | 0.048±0.066 | 0.113±0.052 | -0.068±0.06 | -0.043±0.071 | 0.05±0.047 | 0.078±0.051 |
| -14.6-kyr | $F_{1,170}$=0.539 P=0.46 | **$F_{1,170}$=4.76 P=0.031** | $F_{1,170}$=1.28 P=0.26 | $F_{1,170}$=0.369 P=0.54 | $F_{1,170}$=1.143 P=0.29 | $F_{1,170}$=2.338 P=0.13 |
| lag -3 | 0.111±0.065 | **0.139±0.051** | -0.106±0.06 | **-0.18±0.069** | 0.075±0.046 | 0.083±0.051 |
| -21.9-kyr | $F_{1,170}$=2.894 P=0.091 | **$F_{1,170}$=7.265 P=0.008** | $F_{1,170}$=3.149 P=0.078 | **$F_{1,170}$=6.684 P=0.011** | $F_{1,170}$=2.591 P=0.11 | $F_{1,170}$=2.699 P=0.10 |
| lag -4 | **0.145±0.065** | **0.135±0.051** | **-0.131±0.059** | **-0.28±0.067** | 0.08±0.046 | 0.077±0.051 |
| -29.2-kyr | **$F_{1,170}$=4.977 P=0.027** | **$F_{1,170}$=6.886 P=0.009** | **$F_{1,170}$=4.878 P=0.029** | **$F_{1,170}$=17.313 P<0.001** | $F_{1,170}$=2.969 P=0.087 | $F_{1,170}$=2.291 P=0.13 |
| lag -5 | **0.144±0.065** | **0.102±0.052** | **-0.141±0.059** | **-0.319±0.066** | 0.064±0.046 | 0.06±0.051 |
| -36.5-ky | **$F_{1,170}$=4.919 P=0.028** | **$F_{1,170}$=3.854 P=0.051** | **$F_{1,170}$=5.718 P=0.018** | **$F_{1,170}$=23.35 P<0.001** | $F_{1,170}$=1.886 P=0.17 | $F_{1,170}$=1.419 P=0.24 |
| lag -6 | 0.111±0.065 | 0.039±0.052 | **-0.137±0.059** | **-0.284±0.067** | 0.034±0.046 | 0.029±0.051 |
| -43.8-kyr | $F_{1,170}$=2.925 P=0.089 | $F_{1,170}$=0.568 P=0.45 | **$F_{1,170}$=5.41 P=0.021** | **$F_{1,170}$=18.033 P<0.001** | $F_{1,170}$=0.526 P=0.47 | $F_{1,170}$=0.328 P=0.57 |
| lag -7 | 0.054±0.065 | -0.034±0.052 | **-0.121±0.059** | **-0.186±0.069** | -0.001±0.046 | -0.004±0.051 |
| -51.1-kyr | $F_{1,170}$=0.692 P=0.41 | $F_{1,170}$=0.429 P=0.51 | **$F_{1,170}$=4.192 P=0.042** | **$F_{1,170}$=7.264 P=0.008** | $F_{1,170}$=0.001 P=0.98 | $F_{1,170}$=0.008 P=0.93 |

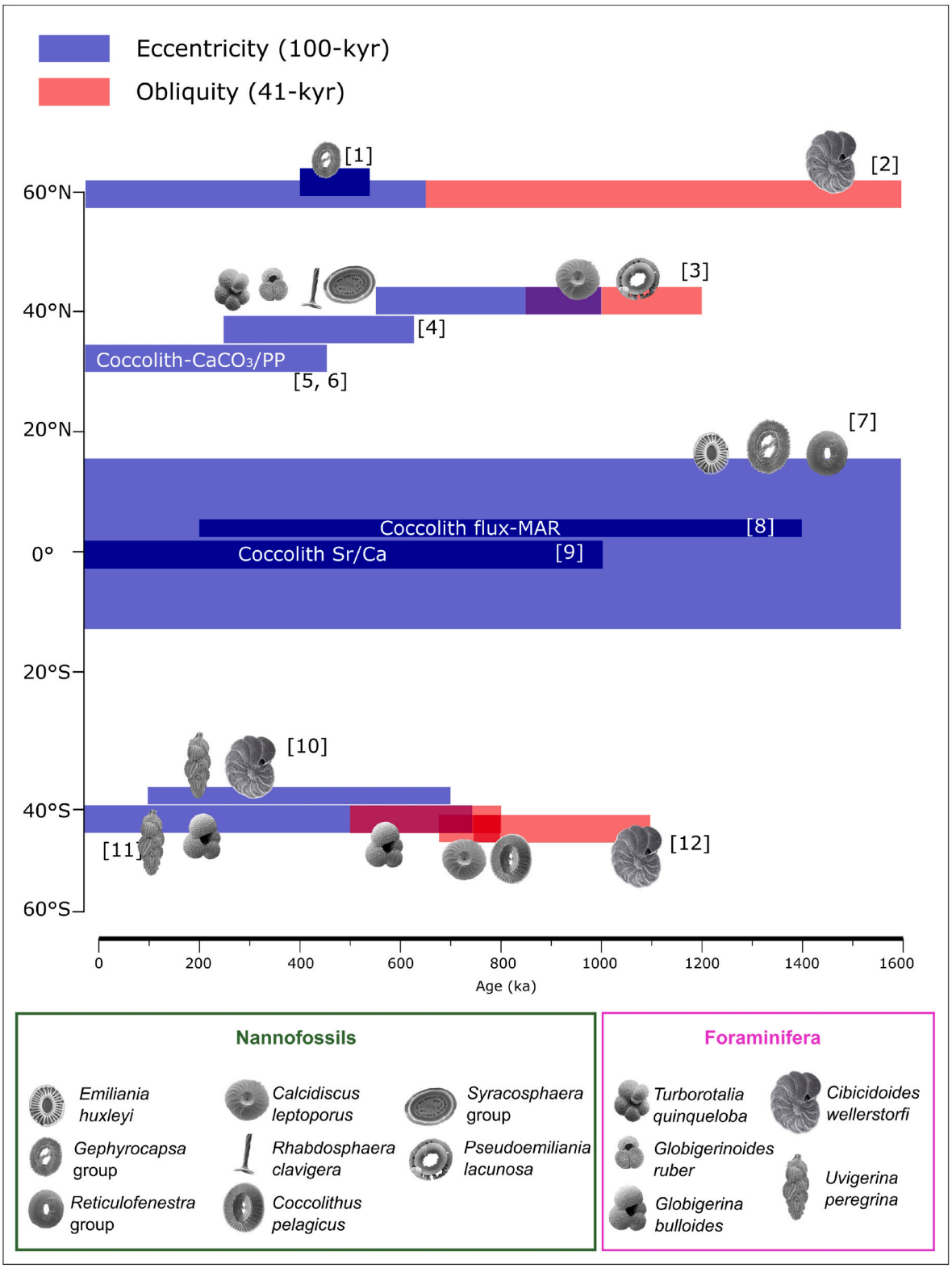


**Fig. 6.** Synopsis of the main orbital signals recorded within the microfossil assemblages and foraminiferal stable isotopes across the last 1.6 Myr. Microfossil photos are indicative of the most significant species recording the main orbital signals (from Young et al., 2022; pforams@mikrotax). For details on species, time-resolution, and studied time intervals of the reported sites see Table S2. Abbreviations: PP - primary productivity index; Coccolith-$CaCO_3$ – calcium carbonate accumulated only from nannofossils; MAR - coccolith mass accumulation rate. References: 1) Martínez-Sánchez et al. (2019); 2) Hodell and Channell (2016); 3) Marino et al. (2008); 4) Maiorano et al. (2016); 5) Bordiga et al. (2014); 6) Bordiga et al. (2013); 7) Beaufort et al. (2022); 8) Jin et al. (2022); 9) Rickaby et al. (2007); 10) Elderfield et al. (2012); 11) Cobianchi et al. (2012); 12) Marino et al. (2009).

environmental processes producing major changes between the pre-MPT and post-MPT oceanic conditions, rather than being affected by higher frequency oscillations such as obliquity dominated G-I cycles. Probably the latitudinal conditions are pivotal, because the studied site is located in the area of the Subtropical Front, and therefore the temperature difference between glacial and interglacial periods is probably not so high as to significantly affect the abundance of nannofossils. Gallagher et al. (2015), through ocean modeling and geochemical analyses of Upper Pleistocene strata (Okinawa Trough and East China Sea) document that the Kuroshio Current path and the Subtropical Front did not change between glacial and interglacial periods and that the glacial/interglacial latitudinal position of the Kuroshio Extension/Polar Front only shifted ~3° southward during glacial maxima.

From the wavelet analysis of L* at ODP Site 1209 it is possible to identify two significant signals: i) a ~100-kyr in the post-MPT signal which can be tentatively connected to the eccentricity orbital component; and ii) an approximately 41-kyr cyclicity related to the Earth's obliquity (Fig. 3C). At Site 1209 L* is associated with the alternation of two main sedimentary components, i.e. the nannofossil oozes (lighter colors) and clay (darker colors). The changes in colour of the core sediments, thus the different L* values, are determined by the combined action of three processes: i) productivity related to the fluxes of pelagic carbonate supply; ii) dilution caused by variations in the terrigenous sediment supply; and iii) dissolution of the carbonate (Einsele and Ricken, 1991). It is possible that at Site 1209 the combination of dilution and dissolution are more strictly related to G-I phases. Indeed, in this area the dilution process shows higher clayey inputs from the Asian continent during the glacials (Zhang et al., 2007), and the dissolution corresponds to the Pacific-style identified by Sexton and Barker (2012) with diminished dissolution during the glacial phases after 1.1 Ma (Bordiga et al., 2014). We cannot exclude a relationship between productivity and G-I cycles, although the six nannofossil species studied here seem to be detached from high-frequency climate cycles.

To date, only a few papers deal with the relationship between nannofossil assemblages and orbital forcing and pacing at mid-latitudes (Beaufort et al., 2022; Bordiga et al., 2013, 2014; Jin et al., 2022; Lupi et al., 2019; Maiorano et al., 2016; Marino et al., 2008, 2009), and further investigations are required to unravel this issue. It should be noted that most existing studies across the MPT interval are based on foraminiferal $\delta^{18}O$ isotopes or taxonomical groups rather than single species and only a few papers inspect the MPT orbital signals derived from single nannofossil species (Table S2). From the few papers available in the literature focusing on all or part of the MPT interval and applying time series analyses to nannofossil assemblages and foraminiferal stable isotope data, it is clear that the equatorial and subtropical latitudes are mainly influenced by orbital eccentricity across the entire MPT (Fig. 6; Table S2). In contrast, at the higher latitudes (i.e. above 40° N and S) where the effect of the ice sheets is predominant, the main recorded periodicity is obliquity which is largely dominant between 600 and 1200 ka, as recorded by both planktonic and benthic foraminifera stable isotope and nannofossil taxa in the Pacific, Southern, and North Atlantic oceans (Fig. 6). The dominance of eccentricity in equatorial-subtropical regions *versus* obliquity at higher latitudes is also reflected in the orbital signals registered by specific species of nannofossils.

### 5.2. Connecting nannofossil paleoecology with orbital pacing

To date, only a few studies of the response of nannofossil species to eccentricity have an adequate resolution across a sufficiently long time period, i.e. more than 1 Myr (Beaufort et al., 2022; Jin et al., 2022; this work). The orbital periodicities recorded within the nannofossil assemblages are often difficult to interpret, especially when it comes to single species level investigations. To amplify and uncover the orbital signals recorded by each nannofossil species across the MPT, previous works applied different power spectral analyses (Marino et al., 2008, 2009) or decomposition of the complex signals into several components representing simpler oscillations on a separated time scale (Intrinsic Mode Functions, IMF; Maiorano et al., 2016). Here, by combining wavelet and statistical time series analyses, we highlight the 100-kyr orbital periodicity recorded in specific taxa (Figs. 4–5). We discuss below how the orbital si gnals as well as the lag (Table 5) recorded by the analyzed species can improve our understanding of the paleoecological preferences of targeted taxa along the MPT time interval.

The abundance fluctuations of some taxa – *C. leptoporus* subsp. *leptoporus*, *G. caribbeanica* small and *Reticulofenestra* spp. (>5 μm) – show a clear lag of 22–40 kyr with respect to the eccentricity oscillation. The negative values of the lags highlighted by the CCF for those species demonstrate the close relationship between eccentricity and nannofossil abundances (Table 3). In contrast, *F. profunda* and *G. ericsonii* are clearly in phase with the eccentricity oscillation, with the latter even returning a positive value of CCF, thus theoretically leading the external forcing (Table 4). This relationship is difficult to interpret because the forcing/pacing itself, and the biosphere response to orbital forcing and climate drivers is complex (Crowhurst et al., 2018) and may entail significant delays due to complex cause-effect connections (Beaufort et al., 2022).

*Calcidiscus leptoporus* subsp. *leptoporus* records an eccentricity response during and immediately following the MPT, with a delay of 37 kyr and higher abundances during eccentricity maxima (Fig. 5A and B; Table 4). Since it is considered a cosmopolitan species, adapted also to cooler water-intermediate temperature and of broad ecological tolerance (Table 2), temperature and latitudinal conditions do not strongly affect its abundance and distribution. In fact, although it is abundant at high latitudes, today *Calcidiscus* populations dominate in the equatorial and subequatorial Pacific (Hagino and Okada, 2006) and in the equatorial Indian Ocean (Renaud et al., 2002), but it is usually rare in the tropical waters of the Atlantic Ocean (e.g. Knappertsbusch et al., 1997; Ziveri et al., 2004). We speculate that this species could be more sensitive than other taxa to the structure of the surface waters. During periods of eccentricity maxima, as mentioned by Beaufort et al. (2022), the strong seasonal contrast (Longhurst, 1998) produces a less homogeneous upper ocean with a more mutable structure leading to an enhancement of more diversified ecological niches (Beaufort et al., 2022).This statement seems to be supported by the nannofossil record, because the H index at Site 1209 shows a major diversity within the nannofossil assemblages during the intervals where *C. leptoporus* subsp. *leptoporus* records its highest abundances as well as the 100-kyr periodicity (Figs. 3–4). Baumann et al. (2016) suggested that *C. leptoporus* subsp. *leptoporus* inhabits preferentially intermediate to deep water with a deep nutricline, and thus when these conditions occur it can proliferate.

*Gephyrocapsa caribbeanica* small shows an anti-correlation with eccentricity during the MPT, starting from 900 ka and also immediately following the MPT, with a delay of 40 kyr, and displays higher abundances during the eccentricity minima (see also Beaufort et al., 2022). This species is indicative of high nutrient water conditions, and in particular the small morphogroup prefers high nutrient and upwelling areas (Table 2). The dominance of its blooms coupled with high coccolithophore production and accumulation in sediments during eccentricity minima are recorded globally (Rickaby et al., 2007). The low seasonality reduces the ecological niches favouring the proliferation of opportunist taxa such as the Noëlaerhabdaceae (Beaufort et al., 2022). Lower values of H index during the maximum abundance of *G. caribbeanica* small confirm the seasonality reduction especially from ca. 600 to 200 ka (Fig. 3).

The *Reticulofenestra* spp. (>5 μm) records eccentricity related variations during and immediately following the MPT, with a delay of 22 kyr, and it displays higher abundances with the eccentricity maxima. The paleoecological preferences of *Reticulofenestra* are still not well known, although in modern assemblages it is considered to be an r-selected life strategy species, proliferating in low salinity, eutrophic and turbulent conditions of coastal and upwelling areas (Table 2). It is

difficult to link the ecological preferences suggested so far to the strong seasonality occurring during eccentricity maxima. This issue may be due to the fact that our data lump within the *Reticulofenestra* group several species that may have different ecological affinities.

*Florisphaera profunda* records a cyclicity of 100 kyr that seems to be in phase with orbital eccentricity (Fig. 5A and B). This deep dweller taxon, abundant when the upper photic zone is nutrient depleted, primarily inhabits subtropical stratified waters (Table 2), and it is influenced more by precession (Beaufort et al., 1997, 2001). Therefore, it is possible that the 100-kyr cyclicity recorded by *F. profunda* is not strictly eccentricity but instead an amplified signal returned by the combination of five precessional cycles (i.e. attributable to "aliasing" or to a "truncated" precessional signal). Unfortunately, the sampling resolution of our current dataset does not allow us to disentangle the orbital signal down to precessional level.

The literature suggests that the results obtained here have a straightforward interpretation in relation to investigations of orbital periodicities on paleoenvironmental indices based on supraspecific taxonomical and morphological categories of nannofossils. These indices measure, for example, paleoproductivity (Beaufort et al., 1997, 2001; Bordiga et al., 2013; Rickaby et al., 2007), $CaCO_3$ accumulation (Beaufort et al., 2022; Bordiga et al., 2014; Marino et al., 2009), dissolution indices (Bordiga et al., 2013; Marino et al., 2009), and morphological divergences (Beaufort et al., 2022). In contrast, when we delve deeply at species-specific levels, it becomes more difficult to return univocal interpretations. This work illustrates that different statistical techniques can help to draw out or highlight different aspects of the data, and can therefore be complementary. Each technique has its own advantages and disadvantages, with the wavelet analysis highlighting more the type of orbital periodicity recorded by different species, and the ACF and CCF disclosing better the consistency of the signal through time as well as the presence of lags. Thus, using complementary sets of techniques (e.g. ACF and CCF or spectral phase estimates, wavelet analyses) can yield better results, especially when it comes to the study of species-specific responses. We also document that the effective orbital drivers impacting the different species are latitude-related, and that those forcings and pacings are recorded only by certain species which are probably influenced by limiting parameters that are strongly orbitally driven or paced.

## 6. Conclusions

We investigated the periodicities recorded by selected nannofossil species across the pre-MPT, MPT, and post-MPT intervals (i.e. over the last 1.6 Myr), and the timing of the biological responses to orbital variations from the mid-latitude ODP Site 1209 (northwest Pacific Ocean). For the first time, different time series analyses, both wavelet and statistical time series (autocorrelation and cross-correlation functions), were applied to the nannofossil abundance datasets, yielding information on species-specific responses to orbital forcing. We documented that most of the selected nannofossil taxa, i.e. *C. leptoporus* subsp. *leptoporus*, *G. caribbeanica* small, *Reticulofenestra* spp. (>5 μm), and *F. profunda,* show 100-kyr cyclicity during the MPT and post-MPT intervals. The species *G. ericsonii*, in contrast, shows two peaks, which are probably the result of the superimposition of two different cycles. The abundance fluctuations of some taxa – *C. leptoporus* subsp. *leptoporus*, *G. caribbeanica* small and *Reticulofenestra* spp. (>5 μm) – show a clear lag of 22–40 kyr with respect to eccentricity. A cause-effect relationship between eccentricity and nannofossil abundances is highlighted by the CCF showing a negative value (equivalent to a positive lag) for the lags. In contrast, the species *F. profunda* and *G. ericsonii* are clearly in phase or lead the eccentricity oscillation as if anticipating higher eccentricity (which is very unlikely) or responding with a long lag to eccentricity minima, or a combination of lags to both eccentricity components. Nannofossil abundances are not always dictated by glacial/interglacial cycles. Across the MPT where the periodicity of the climatic cycles is variable, the nannofossil abundances constantly reflect the eccentricity variations as demonstrated by ACF and CCF. After the 400 ka, we cannot exclude the influence of the G-I cycles, although for the wavelet we are outside the cone of influence.

The orbital signals as well as the lag recorded by the analyzed species enhance understanding of the nannofossil species paleoecological preferences across the MPT time interval. We document that the orbitally forced or paced drivers impacting the species are latitude-related, and that these forcings are recorded particularly well by species (i.e. *C. leptoporus* subsp. *leptoporus*, *G. caribbeanica* small, and *F. profunda*) which are probably more influenced by strongly orbitally driven limiting parameters.

The orbital signal at a species-specific level does not return uniform interpretations, nevertheless, the application of a variety of statistical time series analyses (ACF and CCF) in addition to wavelet analysis permits a better understanding of the relationship between species abundances and orbital forcing.

## Sample credit author statement

Manuela Bordiga: conceptualization, investigation, writing original draft and review & editing. Claudia Lupi: conceptualization, data discussion and review final draft. Roberto Sacchi: statistical analyses and data interpretation. Patrizia Ferretti: methodology and validation. Simon J. Crowhurst: formal analyses. Miriam Cobianchi: conceptualization, writing original draft, head of the project.

## Declaration of competing interest

The authors declare that they have no known competing financial interests or personal relationships that could have appeared to influence the work reported in this paper.

## Data availability

The dataset supporting the findings of this study is available in Zenodo: https://doi.org/10.5281/zenodo.8191622.

## Acknowledgements

The authors are grateful to the International Ocean Discovery Program (IODP) for providing samples to M.C. for this research. The IODP is sponsored by the US National Science Foundation and participating countries. Some of the data used in this study belong to the Ph.D. project of M.B. and it was financially supported by a FAR grant to M.C. (Pavia University) and a Ph.D. grant from MUR (2009–2012) to M.B. This research was also funded through MUR for ECORD-IODP Italia 2018 to M.B within the project "Geochemistry and marine biology united to refine climate models".

## Appendix A. Supplementary data

Supplementary data to this article can be found online at doi: mmcdoino.

## References

Aizawa, C., Oba, T., Okada, H., 2004. Late quaternary paleoceanography deduced from coccolith assemblages in a piston core recovered off the central Japan coast. Mar. Micropaleontol. 52, 277–297.

Ao, H., Dekkers, M.J., Xiao, G., Yang, X., Qin, L., Liu, X., Qiang, X., Chang, H., Zhao, H., 2012. Different orbital rhythms in the Asian summer monsoon records from North and South China during the Pleistocene. Glob. Planet. Change 80– 81, 51–60.

Barkley, R.A., 1970. The Kuroshio current. Sci. J. 6, 54–60.

Baumann, K.-H., Freitag, T., 2004. Pleistocene fluctuations in the northern Benguela Current system as revealed by coccolith assemblages. Mar. Micropaleontol. 52, 195–215.

Baumann, K.-H., Saavedra-Pellitero, M., Böckel, B., Ott, C., 2016. Morphometry, biogeography and ecology of *Calcidiscus* and *umbilicosphaera* in the south atlantic. Rev. Micropaleontol. 59, 239–251.
Beaufort, L., Bolton, C.T., Sarr, A.-C., Suchéras-Marx, B., Rosenthal, Y., Donnadieu, Y., Barbarin, N., Bova, S., Cornuault, P., Gally, Y., Gray, E., Mazur, J.-C., Tetard, M., 2022. Cyclic evolution of phytoplankton forced by changes in tropical seasonality. Nature 601, 79–84.
Beaufort, L., de Garidel-Thoron, T., Mix, A.C., Pisias, N.G., 2001. ENSO-like forcing on oceanic primary production during the Late Pleistocene. Science 293, 2440–2444.
Beaufort, L., Lancelot, Y., Camberin, P., Cayre, O., Vincent, E., Bassinot, F., Labeyrie, L., 1997. Insolation cycles as a major control of equatorial Indian Ocean primary production. Science 278, 1451–1454.
Berends, C.J., Köhler, P., Lourens, L.J., Wal, R.S.W., 2021. On the cause of the mid-pleistocene transition. Rev. Geophys. 59, e2020RG000727.
Berger, W.H., Jansen, E., 1994. Mid-pleistocene climate shift - the nansen connection. In: Johannessen, O.M., Muench, R.D., Overland, J.E. (Eds.), The Polar Oceans and Their Role Shaping the Global Environment. AGU Geophysical Monograph, vol. 85. American Geophysical Union, Washington, D. C., pp. 295–311
Berger, W.H., Winterer, E.L., 1974. Plate stratigraphy and the fluctuating carbonate line. In: Hsü, K.J., Jenkyns, H.C. (Eds.), Pelagic Sediment: on Land and under the Sea, International Sedimentologists Special Publication, vol. 1. Blackwell Publishing Ltd., Oxford, UK, pp. 11–48.
Berger, W.H., Yasuda, M.K., Bickert, T., Wefer, G., Takayama, T., 1994. Quaternary time scale for the ontong java plateau: Milankovitch template for Ocean Drilling Program site 806. Geology 22, 463–467.
Boeckel, B., Baumann, K.-H., Henrich, R., Kinkel, H., 2006. Coccolith distribution patterns in South Atlantic and Southern Ocean surface sediments in relation to environmental gradients. Deep-Sea Res. Part A Oceanogr. Res. Pap. 53, 1073–1099.
Bordiga, M., Bartol, M., Henderiks, J., 2015. Absolute nannofossil abundance estimates: quantifying the pros and cons of different techniques. Rev. Micropaleontol. 58, 155–165.
Bordiga, M., Beaufort, L., Cobianchi, M., Lupi, C., Mancin, N., Luciani, V., Pelosi, N., Sprovieri, M., 2013. Calcareous plankton and geochemistry from the ODP Site 1209B in the NW Pacific Ocean (Shatsky Rise): new data to interpret calcite dissolution and paleoproductivity changes of the last 450 ka. Palaeogeogr. Palaeoclimatol. Palaeoecol. 371, 93–108.
Bordiga, M., Cobianchi, M., Lupi, C., Pelosi, N., Venti, N.L., Ziveri, P., 2014. Coccolithophore carbonate during the last 450 ka in the NW Pacific Ocean (ODP site 1209B, Shatsky Rise). J. Quat. Sci. 29, 57–69.
Bralower, T.J., Premoli Silva, I., Malone, M.J., et al., 2002. Site 1209. In: Bralower, T.J., Premoli Silva, I., Malone, M.J. (Eds.), Proceedings Ocean Drilling Program, Initial Reports, 198. Ocean Drilling Program, College Station TX, pp. 1–102.
Clark, P.U., Alley, R.B., Pollard, D., 1999. Northern Hemisphere ice-sheet influences on global climate change. Science 286, 1104–1111.
Clark, P.U., Archer, D., Pollard, D., Blum, J.D., Rial, J.A., Brovkin, V., Mix, A.C., Pisias, N. G., Roy, M., 2006. The middle Pleistocene transition: characteristics, mechanisms, and implications for long-term changes in atmospheric $pCO_2$. Quat. Sci. Rev. 25, 3150–3184.
Cobianchi, M., Luciani, V., Lupi, C., Mancin, N., Lirer, F., Pelosi, N., Trattenero, I., Bordiga, M., Hall, I.R., Sprovieri, M., 2012. Pleistocene biogeochemical record in the south-west Pacific Ocean (images site MD97-2114, chatham Rise). J. Quat. Sci. 27, 519–530.
Crowhurst, S.J., Pälike, H., Rickaby, R.E.M., 2018. Carbonate ions, orbits and Mg/Ca at ODP 1123. Geochem. Cosmochim. Acta 236, 384–398.
de Garidel-Thoron, T., Rosenthal, Y., Bassinot, F., Beaufort, L., 2005. Stable sea surface temperatures in the western Pacific warm pool over the past 1.75 million years. Nature 433, 294–298.
Diekmann, B., Kuhn, G., 2002. Sedimentary record of the mid-Pleistocene climate transition in the southeastern South Atlantic (ODP Site 1090). Palaeogeogr. Palaeoclimatol. Palaeoecol. 182, 241–258.
Einsele, G., Ricken, W., 1991. In: Einsele, G., Ricken, W., Seilacher, A. (Eds.), Limestone-Marl Alternations. Springer-Verlag, pp. 23–48.
Elderfield, H., Ferretti, P., Greaves, M., Crowhurst, S., McCave, I.N., Hodell, D., Piotrowski, A.M., 2012. Evolution of ocean temperature and ice volume through the Mid-Pleistocene Climate Transition. Science 337, 704–709.
EPICA community members, 2004. Eight glacial cycles from an Antarctic ice core. Nature 429, 623–628.
Flores, J.A., Filippelli, F.J., Bárcena, G.M., Pérez-Folgado, M.Á., Vázquez, M., Utrlilla, A., 2005. Surface water dynamics and hytoplankton communitiesduring deposition of cyclic late Messinian sapropel sequences in the western Mediterranean. Mar. Micropaleontol. 56, 50–79.
Flores, J.A., Gersonde, R., Sierro, F.J., 1999. Pleistocene fluctuations in the Agulhas Current retroflection based on the calcareous plankton record. Mar. Micropaleontol. 37, 1–22.
Flores, J.-A., Gersonde, R., Sierro, F.J., Niebler, H.-S., 2000. Southern Ocean Pleistocene calcareous nannofossil events: calibration with isotope and geomagnetic stratigraphies. Mar. Micropaleontol. 40, 377–402.
Ford, H.L., Raymo, M.E., 2019. Regional and global signals in seawater $\delta^{18}O$ records across the mid-Pleistocene transition. Geology 48, 113–117.
Gallagher, S.J., Kitamura, A., Iryu, Y., Itaki, T., Koizumi, I., Hoiles, P.W., 2015. The Pliocene to recent history of the Kuroshio and Tsushima Currents: a multi-proxy approach. Prog. Earth Planet. Sci. 2, 17.
Hagino, K., Okada, H., 2006. Intra- and infra-specific morphological variation in selected coccolithophore species in the equatorial and subequatorial Pacific Ocean. Mar. Micropaleontol. 58, 184–206.
Haug, G.H., Maslin, M.A., Sarnthein, M., Stax, R., Tiedemann, R., 1995. Evolution of northwest Pacific sedimentation patterns since 6 Ma (site 882). In: Rea, D.K., Basov, La, Scholl, D.W., Allan, J.F. (Eds.), Proceedings of the Ocean Drilling Program, 145 Scientific Results, 145. Ocean Drilling Program, College Station, TX, pp. 293–301.
Hodell, D.A., Channell, J.E.T., 2016. Mode transitions in Northern Hemisphere glaciation: Co-evolution of millennial and orbital variability in Quaternary climate. Clim. Past 12, 1805–1828.
Hu, D., Wu, L., Cai, W., Gupta, A.S., Ganachaud, A., Qiu, B., Gordon, A.L., Lin, X., Chen, Z., Hu, S., Wang, G., Wang, Q., Sprintall, J., Qu, T., Kashino, Y., Wang, F., Kessler, W.S., 2015. Pacific western boundary currents and their roles in climate. Nature 522, 299–308.
Huybers, P., Wunsch, C., 2005. Obliquity pacing of the late Pleistocene glacial terminations. Nature 434, 491–494.
Jin, X., Ma, W., Liu, C., 2022. Origin of the long-term increase in coccolith size and its implication for carbon cycle and climate over the past 2 Myr. Quat. Sci. Rev. 290, 107642.
Jouzel, J., Masson-Delmotte, V., Cattani, O., Dreyfus, G., Falourd, S., Hoffmann, G., Minster, B., Nouet, J., Barnola, J.M., Chappellaz, J., Fischer, H., Gallet, J.C., Johnsen, S., Leuenberger, M., Loulergue, L., Luethi, D., Oerter, H., Parrenin, F., Raisbeck, G., Raynaud, D., Schilt, A., Schwander, J., Selmo, E., Souchez, R., Spahni, R., Stauffer, B., Steffensen, J.P., Stenni, B., Stocker, T.F., Tison, J.L., Werner, M., Wolff, E.W., 2007. Orbital and millennial Antarctic climate variability over the past 800,000 years. Science 317, 793–796.
Kawahata, H., Ohkushi, K.-I., Hatakeyama, Y., 1999. Comparative late Pleistocene paleoceanographic changes in the mid latitude boreal and austral western pacific. J. Oceanogr. 55, 747–761.
Kawahata, H., Ohshima, H., 2002. Small latitudinal shift in the Kuroshio Extension (Central Pacific) during glacial times: evidence from pollen transport. Quat. Sci. Rev. 21, 1705–1717.
Kitamura, A., Kawagoe, T., 2006. Eustatic sea-level change at the Mid-Pleistocene climate transition: new evidence from the shallow-marine sediment record of Japan. Quat. Sci. Rev. 25, 323–335.
Kleijne, A., 1993. Morphology, Taxonomy and Distribution of the Extant Coccolithophorids (Calcareous Nannoplankton). Ph.D. Thesis). Vrije Universiteit, Amsterdam, p. 321.
Knappertsbusch, M., Cortes, M.Y., Thierstein, H.R., 1997. Morphologic variability of the coccolithophorid *Calcidiscus leptoporus* in the plankton, surface sediments and from the Early Pleistocene. Mar. Micropaleontol. 30, 293–317.
Laskar, J., Fienga, A., Gastineau, M., Manche, H., 2011. La2010: a new orbital solution for the long-term motion of the Earth. Astron. Astrophys. 532, A89.
Lee, S.-Y., Poulsen, C.J., 2005. Tropical Pacific climate response to obliquity forcing in the Pleistocene. Paleoceanography 20, PA4010.
Lisiecki, L.E., Raymo, M.E., 2007. Plio–Pleistocene climate evolution: trends and transitions in glacial cycle dynamics. Quat. Sci. Rev. 26, 56–69.
Lisiecki, L.E., Raymo, M.E., 2005. A Pliocene-Pleistocene stack of 57 globally distributed benthic $\delta^8O$ records. Paleoceanography 20, PA1003.
Liu, H., Suzuki, K., Saito, H., 2004. Community structure and dynamics of phytoplankton in the western subarctic Pacific Ocean: a synthesis. J. Oceanogr. 60, 119–137.
Longhurst, A., 1998. Ecological Geography of the Sea, vol. 1. Academic Press.
López-Otálvaro, G.-E., Flores, J.-A., Sierro, F.J., Cacho, I., 2008. Variations in coccolithophorid production in the Eastern Equatorial Pacific at ODP Site 1240 over the last seven glacial–interglacial cycles. Mar. Micropaleontol. 69, 52–69.
Lupi, C., Bordiga, M., Cobianchi, M., 2012. *Gephyrocapsa* occurrence during the middle Pleistocene transition in the northern Pacific Ocean (Shatsky Rise). Geobios 45, 209–217.
Lupi, C., Bordiga, M., Sacchi, R., Ferretti, P., Cobianchi, M., 2019. Calcareous nannofossil response to climate variability during the middle Pleistocene transition in the northwest Pacific ocean (Ocean Drilling Program leg 198 site 1209). Paleoceanogr. Paleoclimatology 34, 600–615.
Maiorano, P., Girone, A., Marino, M., Kucera, M., Pelosi, N., 2016. Sea surface water variability during the Mid-Brunhes inferred from calcareous plankton in the western Mediterranean (ODP Site 975). Palaeogeogr. Palaeoclimatol. Palaeoecol. 459, 229–248.
Maiorano, P., Marino, M., 2004. Calcareous nannofossil bioevents and environmental control on temporal and spatial patterns at the early–middle Pleistocene. Mar. Micropaleontol. 53, 405–422.
Maiorano, P., Tarantino, F., Marino, M., De Lange, G.J., 2013. Paleoenvironmental conditions at core KC01B (ionian sea) through MIS 13–9: evidence from calcareous nannofossil assemblages. Quat. Int. 288, 97–111.
Maraun, D., Kurths, J., 2004. Cross wavelet analysis: significance testing and pitfalls. Nonlinear Process Geophys. 11, 505–514.
Maraun, D., Kurths, J., Holschneider, M., 2007. Nonstationary Gaussian processes in wavelet domain: synthesis, estimation, and significance testing. Phys. Rev. E 75, 016707.
Marino, M., Maiorano, P., Lirer, F., 2008. Changes in calcareous nannofossil assemblages during the Mid-Pleistocene Revolution. Mar. Micropaleontol. 69, 70–90.
Marino, M., Maiorano, P., Lirer, F., Pelosi, N., 2009. Response of calcareous nannofossil assemblages to paleoenvironmental changes through the mid-Pleistocene revolution at Site 1090 (Southern Ocean). Palaeogeogr. Palaeoclimatol. Palaeoecol. 280, 333–349.
Martínez-Sánchez, M., Flores, J.-A., Palumbo, E., Alonso-Garcia, M., Sierro, F.-J., Amore, F.O., 2019. Reconstruction of surface water dynamics in the North Atlantic during the Mid-Pleistocene (~540–400 ka), as inferred from coccolithophores and planktonic foraminifera. Mar. Micropaleontol. 152, 101730.

McClymont, E.L., Sosdian, S.M., Rosell-Melé, A., Rosenthal, Y., 2013. Pleistocene sea-surface temperature evolution: early cooling, delayed glacial intensification, and implications for the mid-Pleistocene climate transition. Earth Sci. Rev. 123, 173–193.
Medina-Elizalde, M., Lea, D.W., 2005. The mid-pleistocene transition in the tropical pacific. Science 310, 1009–1012.
Molfino, B., McIntyre, A., 1990. Nutricline variation in the equatorial atlantic coincident with the younger dryas. Paleoceanography 5, 997–1008.
Mudelsee, M., Schulz, M., 1997. The Mid-Pleistocene climate transition: onset of 100 ka cycle lags ice volume build-up by 280 ka. Earth Planet Sci. Lett. 151, 117–123.
Okada, H., Honjo, S., 1973. The distribution of oceanic coccolithophorids in the Pacific. Deep Sea Res. 20, 355–374.
Okada, H., McIntyre, A., 1979. Seasonal distribution of modern coccolithophores in the western North Atlantic Ocean. Mar. Biol. 54, 319–328.
Pena, L.D., Goldstein, S.L., 2014. Thermohaline circulation crisis and impacts during the mid-Pleistocene transition. Science 345, 318–322.
Petit, J.R., Jouzel, J., Raynaud, D., Barkov, N.I., Delaygue, G., Delmotte, M., Kotlyakov, V.M., Legrand, M., Lipenkov, V.Y., Lorius, C., Saltzman, E., 1999. Climate and atmospheric history of the past 420,000 years from the Vostok ice core, Antarctica. Nature 399, 429–436.
pforams@mikrotax. https://www.mikrotax.org/pforams/. (Accessed 14 March 2023).
Pisias, N.G., Moore, T.C., 1981. The evolution of Pleistocene climate: a time series approach. Earth Planet Sci. Lett. 52, 450–458.
Prell, W.L., 1982. Oxygen and carbon isotopic stratigraphy for the Quaternary of Hole 502B: evidence for two modes of isotopic variability. In: Prell, W.L., Gardner, J.V., et al. (Eds.), Initial Reports of the Deep Sea Drilling Project, vol. 68. U.S. Government Printing Office, Washington, pp. 455–464.
Qiu, B., 2002. The Kuroshio Extension system: its large-scale variability and role in the Midlatitude Ocean-Atmosphere interaction. J. Oceanogr. 58, 57–75.
Qiu, B., 2001. Kuroshio and Oyashio currents. In: Steele, J.H., Turekian, K.K., et al. (Eds.), Encyclopedia of Ocean Sciences. Reference Module in Earth Systems and Environmental Sciences. Elsevier, pp. 1413–1425.
Qiu, B., 2000. Interannual variability of the Kuroshio Extension system and its impact on the wintertime SST field. J. Phys. Oceanogr. 30, 1486–1502.
R Core Team, 2020. R: A Language and Environment for Statistical Computing. R Foundation for Statistical Computing, Vienna, Austria. https://www.R-project.org/.
Renaud, S., Ziveri, P., Broerse, A.T.C., 2002. Geographical and seasonal differences in morphology and dynamics of the coccolithophore *Calcidiscus leptoporus*. Mar. Micropaleontol. 46, 363–385.
Rickaby, R.E.M., Bard, E., Sonzogni, C., Rostek, F., Beaufort, L., Barker, S., Rees, G., Schrag, D.P., 2007. Coccolith chemistry reveals secular variations in the global ocean carbon cycle? Earth Planet Sci. Lett. 253, 83–95.
Ruddiman, W.F., Raymo, M.E., McIntyre, A., 1986. Matuyama 41,000-year cycles: north Atlantic Ocean and northern hemisphere ice sheets. Earth Planet Sci. Lett. 80, 117–129.
Saavedra-Pellitero, M., Flores, J.-A., Baumann, K.-H., Sierro, F.-J., 2010. Coccolith distribution patterns in surface sediments of equatorial and southeastern Pacific Ocean. Geobios 43, 131–149.
Sancetta, C., Silvestri, S., 1986. Pliocene-Pleistocene evolution of the North Pacific Ocean-Atmosphere system, interpreted from fossil diatoms. Paleoceanography 1, 163–180.
Sasai, Y., 2007. Seasonal and intra-seasonal variability of chlorophyll-a in the North Pacific: model and satellite data. J. Earth Simulator 8, 3–11.
Sexton, P.F., Barker, S., 2012. Onset of 'Pacific-style' deep-sea sedimentary carbonate cycles at the mid-Pleistocene transition. Earth Planet Sci. Lett. 321–322, 81–94.
Shackleton, N.J., Berger, A., Peltier, W.R., 1990. An alternative astronomical calibration of the lower Pleistocene timescale based on ODP Site 677. Trans. R. Soc. Edinb. Earth Sci. 81, 251–261.
Shackleton, N.J., Opdyke, N.D., 1976. Oxygen-isotope and paleomagnetic stratigraphy of pacific core V28-239: late pliocene to latest Pleistocene. Geol. Soc. Am. Mem. 145, 449–464.
Siegenthaler, U., Stocker, T.F., Monnin, E., Luthi, D., Schwander, J., Stauffer, B., Raynaud, D., Barnola, J.-M., Fischer, H., Masson-Delmotte, V., Jouzel, J., 2005. Stable carbon cycle - climate relationship during the late Pleistocene. Science 310, 1313–1317.
Sprengel, C., Baumann, K.-H., Henderiks, J., Henrich, R., Neuer, S., 2002. Modern coccolithophore and carbonate sedimentation along a productivity gradient in the Canary Islands region: seasonal export production and surface accumulation rates. Deep Sea Res. Part II 49, 3577–3598.
Stirnemann, J.M., Bühlmann, R., 2021. Worldmapgenerator. https://www.worldmapgenerator.com/en/.
Stoffer, D., 2020. Astsa: Applied Statistical Time Series Analysis. R package version 1.12. https://CRAN.R-project.org/package=astsa.
Tabor, C.R., Poulsen, C.J., Pollard, D., 2015. How obliquity cycles powered early Pleistocene global ice-volume variability. Geophys. Res. Lett. 42, 1871–1879.
Thompson, P.R., 1981. Planktonic foraminifera in the Western North Pacific during the past 150 000 years: comparison of modern and fossil assemblages. Palaeogeogr. Palaeoclimatol. Palaeoecol. 35, 241–279.
Thompson, P.R., Shackleton, N.J., 1980. North Pacific palaeoceanography: late Quaternary coiling variations of planktonic foraminifer *Neogloboquadrina pachyderma*. Nature 287, 829–833.
Trapletti, A., Hornik, K., 2020. Tseries: Time Series Analysis and Computational Finance. R Package Version 0.10-48. https://CRAN.R-project.org/package=tseries.
Trujillo, A.P., Thurman, H.V., 2011. Essentials of Oceanography, tenth ed. Prentice Hall, Boston, pp. 161–192.
Usui, N., Tsujino, H., Nakano, H., Matsumoto, S., 2013. Long-term variability of the Kuroshio path south of Japan. J. Oceanogr. 69, 647–670.
Vincent, E., 1975. Neogene planktonic foraminifera from the central north pacific, leg 32, Deep Sea Drilling Project. In: Larson, R.L., Moberly, R., et al. (Eds.), Initial Reports of the Deep Sea Drilling Project, vol. 32. U.S. Government Printing Office, Washington, DC, pp. 765–801.
Weirauch, D., Billups, K., Martin, P., 2008. Evolution of millennial-scale climate variability during the mid-Pleistocene. Paleoceanography 23, PA3216.
Westerhold, T., Röhl, U., 2006. Data report: revised composite depth records for Shatsky Rise sites 1209, 1210, and 1211. In: Proceedings of the Ocean Drilling Program, Scientific Results, vol. 198. Ocean Drilling Program, College Station TX, pp. 1–26.
Winter, A., 1982. Paleoenvironmental interpretation of quaternary coccolith assemblages from the gulf of aqaba (elat), red sea. Rev. Espanola Micropaleontol. 14, 291–314.
Winter, A., Jordan, R.W., Roth, P.H., 1994. Biogeography of living coccolithophores in ocean waters. In: Winter, A., Siesser, W.G. (Eds.), Coccolithophores: from Molecular Processes to Global Impact. Cambridge University Press, Cambridge, UK, Cambridge, UK, pp. 161–177.
Young, J.R., 1994. The functions of coccoliths. In: Winter, A., Siesser, W.G. (Eds.), Coccolithophores. Cambridge University Press, London, pp. 63–82.
Young, J.R., Bown, P.R., Lees, J.A., 2022. Nannotax3 Website. International Nannoplankton Association. www.mikrotax.org/Nannotax3. (Accessed 21 April 2022).
Zhang, J., Wang, P., Li, Q., Cheng, X., Zhang, S., 2007. Western equatorial Pacific productivity and carbonate dissolution over the last 550 kyr: foraminiferal and nannofossil evidence from ODP Hole 807A. Mar. Micropaleontol. 64, 121–140.
Ziveri, P., Baumann, K.-H., Boeckel, B., Bollmann, J., Young, J., 2004. Biogeography of selected holocene coccoliths in the Atlantic Ocean. In: Thierstein, H.R., Young, J. (Eds.), Coccolithophores from Molecular Processes to Global Impact. Springer, Berlin, pp. 400–452.